

## STUDY OF NUCLEAR STRUCTURE WITH QUASIELASTIC PROTON SCATTERING AT 1 GeV

Yu.V.Dotsenko, A.A.Vorobyov

The modern microscopic nuclear theories are based on the concept of independent particle motion in a self-consistent field resulted from the effective nucleon-nucleon interactions. Therefore, experimental studies of the nuclear shell structure are of special interest. Here we present a short review of the experiments on quasielastic proton-nucleon scattering carried out at the PNPI synchrocyclotron in the period 1985–1995.

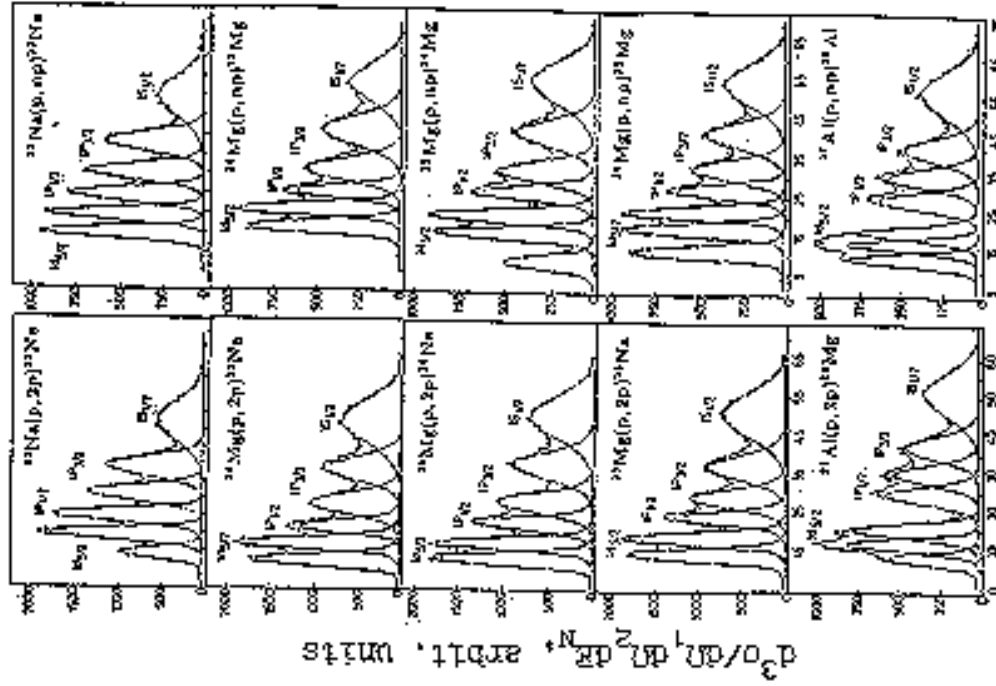
The experiments were performed using a correlation missing-mass spectrometer with the total energy resolution of 3.5 MeV (FWHM), the proton beam energy being 1000 MeV.

The  $(p, 2p)$  and  $(p, np)$  reactions were studied in identical conditions: the scattered proton was detected with a magnetic spectrometer, while the knocked out nucleon ( $p$  or  $n$ ) was detected with a time-of-flight spectrometer. The measurements have been done with the following isotopically enriched targets [1–7]:  ${}^6\text{Li}$ ,  ${}^7\text{Li}$ ,  ${}^9\text{Be}$ ,  ${}^{10}\text{B}$ ,  ${}^{11}\text{B}$ ,  ${}^{12}\text{C}$ ,  ${}^{16}\text{O}$ ,  ${}^{23}\text{Na}$ ,  ${}^{24}\text{Mg}$ ,  ${}^{25}\text{Mg}$ ,  ${}^{26}\text{Mg}$ ,  ${}^{27}\text{Al}$ ,  ${}^{28}\text{Si}$ ,  ${}^{29}\text{Si}$ ,  ${}^{30}\text{Si}$ ,  ${}^{31}\text{P}$ ,  ${}^{32}\text{S}$ ,  ${}^{34}\text{S}$ ,  ${}^{39}\text{K}$ ,  ${}^{40}\text{Ca}$ ,  ${}^{90}\text{Zr}$ ,  ${}^{208}\text{Pb}$ . The goal of these investigations was to study the shell structure of these nuclei, especially the inner proton and neutron shells including the  $1s_{1/2}$  shell. Prior to our measurements, the neutron shells energies were in most cases unknown. In some cases, the proton shell parameters were also unknown or required more precise measurements, in particular for strongly bound states which could not be investigated in the low energy experiments.

One important result of these studies was the observation of the  $1s_{1/2}$  and  $1p_{1/2}$  proton and neutron shells in all nuclei up to  ${}^{90}\text{Zr}$  and  ${}^{208}\text{Pb}$ . The  $A$ -dependence of the shell energies is a sensitive test of the effective  $NN$  interactions chosen for generation of the self-consistent nuclear field (see discussion below). In particular, our data demonstrate the saturation effect in the nucleon binding energies with the increase of  $A$ .

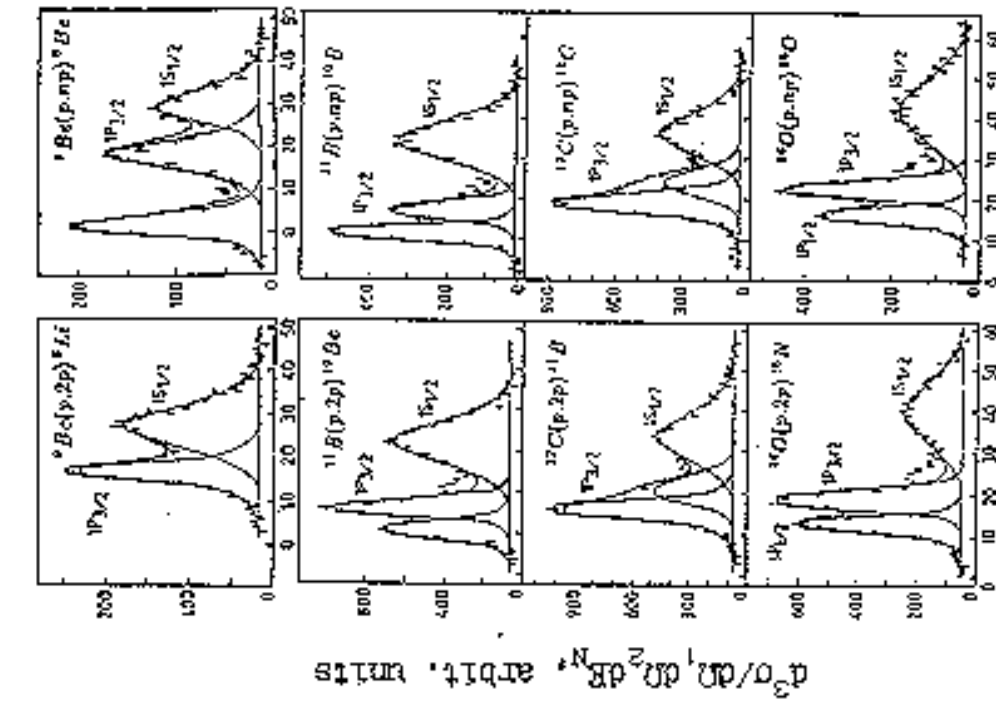
The most remarkable is the observation of the shell splitting in many of the studied nuclei. This splitting is revealed first in the neutron separation energy spectrum in  ${}^9\text{Be}$  (Fig. 1a). Besides two peaks that could be identified as the  $1s$  and  $1p$  states, an additional peak appeared at low binding energy. This peak can be interpreted as splitting of the  $1p_{3/2}$  shell into two states. Similar splitting of the  $1p$  shell is clearly seen in  ${}^{10}\text{B}$ ,  ${}^{11}\text{B}$ , and  ${}^{12}\text{C}$ , both in the neutron and proton shells (Fig. 1a).

Even more pronounced picture is observed in the nuclei with  $2s$ – $1d$  shells (Fig. 1b, 2). In addition to the splitting of the  $1p_{3/2}$  shell, in this case one can see also splitting of the  $1d_{5/2}$  shell into three states with two protons (neutrons) in each state. This shell structure is conserved in  ${}^{29,30}\text{Si}$ ,  ${}^{31}\text{P}$ ,  ${}^{32}\text{S}$ , where one can see also the appearance of the  $2s_{1/2}$  state. Further increase of the nuclear mass reduces the distances between the splitted peaks so that in  ${}^{39}\text{K}$  the splitting is hardly seen at the level of the resolution reached in our experiment. Finally, we should point out that the shell structure in the magic nuclei ( ${}^{16}\text{O}$ ,  ${}^{40}\text{Ca}$ ,  ${}^{90}\text{Zr}$ ,  ${}^{208}\text{Pb}$ ) corresponds to the simple shell model without noticeable shell splitting and with the shell filling by the nucleons according to the  $(2j + 1)$  rule.



Separation Energy  $E_{N^+}$ , MeV

Fig. 1a. Separation energy spectra for  ${}^9\text{Be}$ ,  ${}^{11}\text{B}$ ,  ${}^{12}\text{C}$ , and  ${}^{16}\text{O}$ .



Separation Energy  $E_{N^+}$ , MeV

Fig. 1b. Separation energy spectra for  ${}^{23}\text{Na}$ ,  ${}^{24}\text{Mg}$ ,  ${}^{25}\text{Mg}$ , and  ${}^{27}\text{Al}$ .

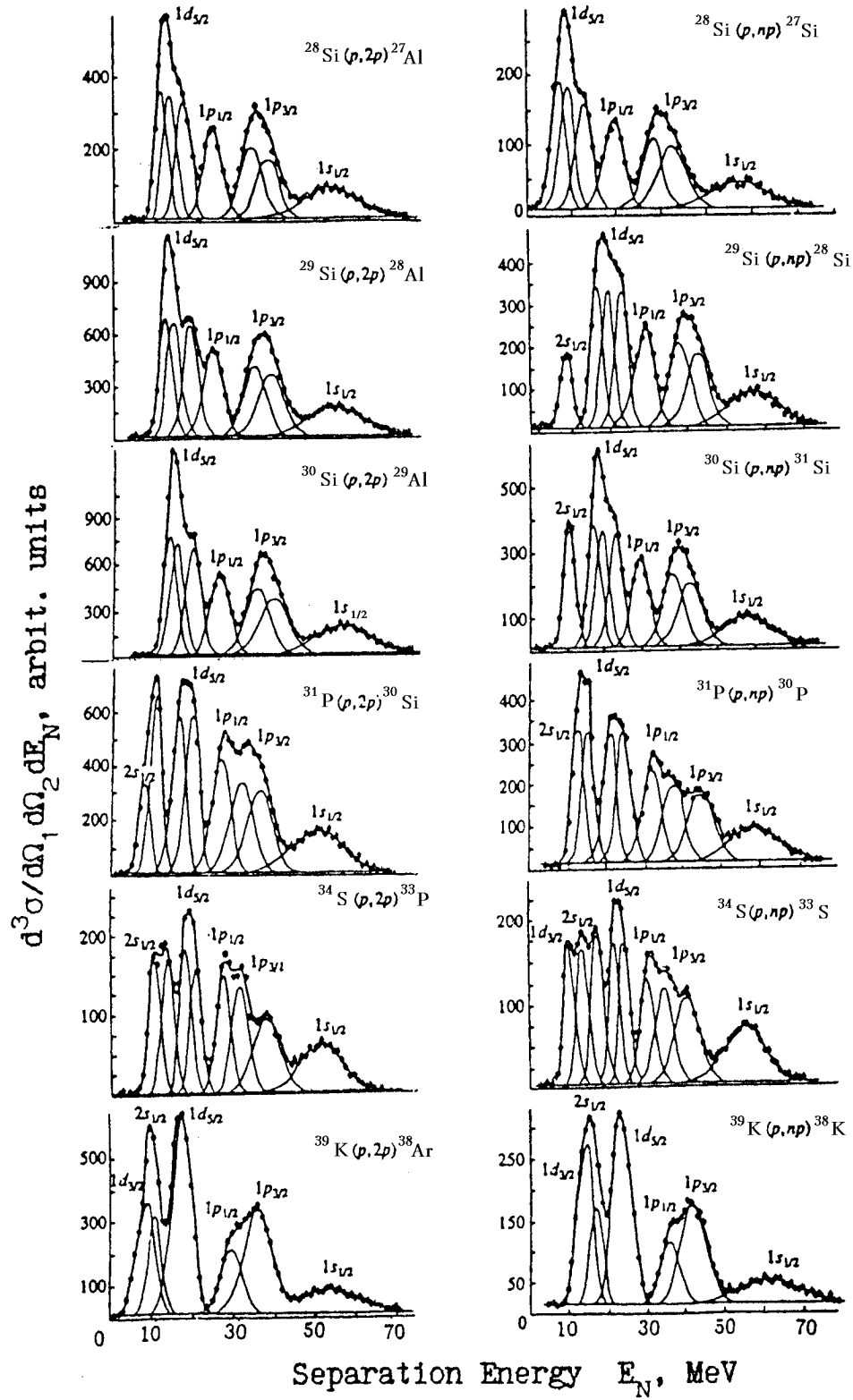
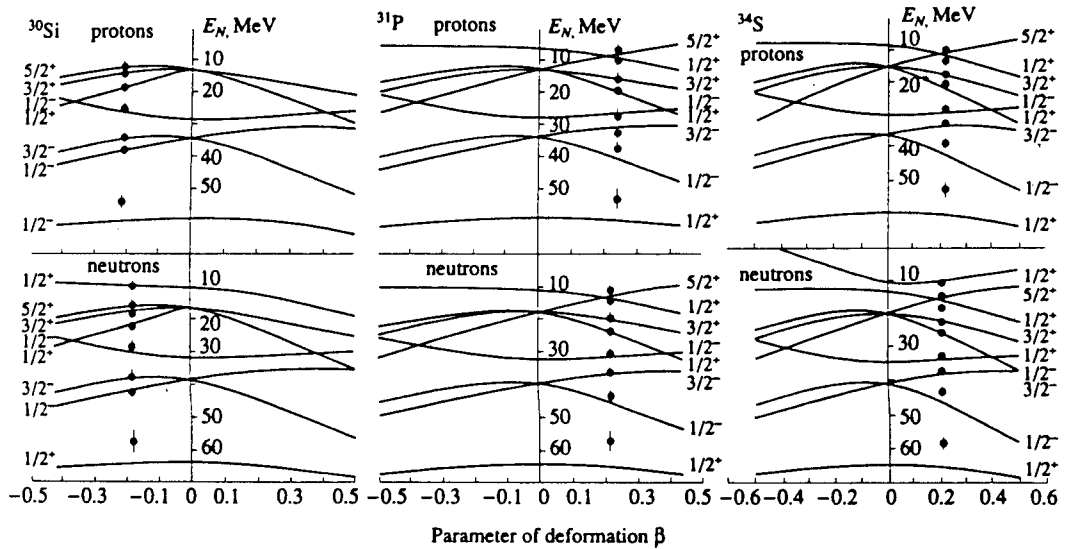


Fig. 2. Nucleon separation energy spectra for  $^{28,29,30}\text{Si}$ ,  $^{31}\text{P}$ ,  $^{32,34}\text{S}$ , and  $^{39}\text{K}$ .

Thus, most of the studied nuclei (except the magic nuclei and  $^{39}\text{K}$ ) reveal the shell structure that could be interpreted by splitting of the  $1p_{3/2}$  and  $1d_{5/2}$  shells into two and three states, respectively. We have proposed that such splitting may take place due to spatial deformation of the self-consistent nuclear field [2]. The axially deformed field conserves the projections of the nucleon momenta on to the symmetry axis in the nucleus, so the quantum numbers of the nucleon states become  $\Omega^\pi$ , and the  $1p_{3/2}$  and  $1d_{5/2}$  shells will be splitted, accordingly, into two and three states with the maximum nucleon occupancy numbers  $\eta_p = \eta_n = 2$ . The energies of the states (and also splitting) depend on the magnitude and the sign of the deformation that opens a unique possibility to study the deformation parameters of the nuclear field seen both by protons and by neutrons. Also, it becomes possible to determine the sign of the deformation. This is qualitatively illustrated by Fig. 3 showing the dependence of the nucleon energy states ( $E_p, E_n$ ) on the deformation parameter  $\beta_2$  calculated using a simple single-particle model. One can see that the agreement between the measured energies  $E_p$  and  $E_n$  and the calculated ones can be reached by choosing certain values of the  $\beta_2$ -parameter, this parameter being positive in  $^{31}\text{P}$  and  $^{32}\text{S}$  and negative in  $^{30}\text{Si}$ . Note also that the neutron and proton deformation parameters proved to be identical.



**Fig. 3.** The energies of single-particle states of protons and neutrons in  $^{30}\text{Si}$ ,  $^{31}\text{P}$ , and  $^{34}\text{S}$  as functions of the deformation parameter. The positions of the experimental points correspond to the optimal values of  $\beta_{2p}$  and  $\beta_{2n}$ .

For quantitative analysis of the obtained data we have developed a "partially self-consistent nuclear model" [2] on the base of the Hartree–Fock method with the Skyrme-type  $NN$  forces. In this model, the quadrupole and hexadecupole deformation parameters  $\beta_{2q}$  and  $\beta_{4q}$  appear in the Hamiltonian in the following way:

$$H^q(r) = H_0^q(r) + R\{\beta_{2q} \cdot Y_{20}(\Theta) + \beta_{4q} Y_{40}(\Theta)\} \cdot dU_q(r)/dr, \quad q = p, n.$$

Here  $H_0^q(r)$  is a spherical Hartree–Fock Hamiltonian with the Skyrme forces,  $U_q(r)$  is its central part,  $R = 1.4(A - 1)^{1/3}$  fm is the radius of the nucleus. In solution of the Schrödinger equation, the single-particle wave functions were determined by diagonalization of the  $H^q(r)$ -matrix

on the basis of the eigenfunctions of the spherical Hamiltonian  $H_0^q(r)$ . The deformation parameters were found through the best fit to the experimental nucleon separation energies. This procedure made it possible also to determine the sign of the deformation due to different behaviour of the single-particle orbitals for prolate and oblate shapes of the nucleus (Fig. 3). The single-particle wave functions corresponding to the resulting deformation parameters were used then to reconstruct the nuclear wave function (as the Slater determinant) and to calculate some nuclear parameters by averaging the corresponding operators.

The obtained proton, neutron, and nuclear matter quadrupole moments ( $Q_{2p}, Q_{2n}, Q_{2m}$ ) are presented in Table. For comparison, the charge quadrupole moments  $Q_{ch}$  measured in other experiments (M.P. Avotina, A.V. Zolotavin, "Ground and excited states nuclear moments", Atomizdat, V.1, 1979) are also presented in Table.

Table

Nucleus	$Q_{2p}$ fm <sup>2</sup>	$Q_{ch}$ fm <sup>2</sup>	$Q_{2n}$ fm <sup>2</sup>	$Q_{2m}$ fm <sup>2</sup>
<sup>6</sup> Li	+2.6(1.7)	+1.3(1.3)	+2.5(1.8)	+5.1(2.5)
<sup>7</sup> Li	+7.2(2.1)	+7.2(2.5)	+12.3(2.5)	+19.8(3.3)
<sup>9</sup> Be	+15.8(2.6)	+16.5(2.5)	+17.3(2.7)	+33.1(3.6)
<sup>10</sup> B	+15.5(3.2)	+16.2(3.1)	+15.7(3.0)	+31.2(4.5)
<sup>11</sup> B	+11.6(3.5)	+18.0(3.5)	+11.0(3.6)	+22.6(4.9)
<sup>12</sup> C	-18.5(5.1)	-20.5(1.5)	-19.0(5.5)	-37.5(7.1)
<sup>23</sup> Na	+45.3(3.2)		+43.0(4.0)	+88.3(6.3)
<sup>24</sup> Mg	+45.8(5.0)	+53.5(2.1)	+50.7(4.9)	+96.5(7.0)
<sup>25</sup> Mg	+48.9(4.8)	+57.3	+52.8(5.1)	+101.7(7.0)
<sup>26</sup> Mg	+49.6(4.6)	+44.0(3.0)	+63.9(4.5)	+113.5(5.3)
<sup>27</sup> Al	+33.4(4.2)	+24.5	+32.5(4.7)	+65.9(5.3)
<sup>28</sup> Si	-48.5(6.1)	-47.0(2.0)	-49.3(6.9)	-98.8(8.1)
<sup>29</sup> Si	-47.7(2.4)		-43.4(2.7)	-91.1(3.6)
<sup>30</sup> Si	-48.9(3.2)		-48.0(3.8)	-86.9(4.8)
<sup>31</sup> P	+54.3(2.4)		+53.9(2.4)	+108.2(2.4)
<sup>32</sup> S	+58.7(5.5)	+53.0	+59.9(4.6)	+118.6(7.0)
<sup>34</sup> S	+50.4(5.0)		+48.2(4.9)	+98.6(7.0)

The agreement between  $Q_{ch}$  and  $Q_{2p}$  is quite satisfactory. So we may be sure that the neutron quadrupole moments are also reliably determined in our experiments. Note that the neutron quadrupole moments have been determined for the first time. The comparison of  $Q_{2n}$  with  $Q_{2p}$  shows that the neutron and proton field deformations are very close to each other in all studied nuclei (with, perhaps, one exception of <sup>7</sup>Li).

To analyze the  $A$ -dependence of the nucleon separation energies, we applied the self-consistent Hartree–Fock microscopic theory to axially deformed nuclei with the effective Skyrme  $NN$  forces. Fig. 4 demonstrates the calculated separation energies  $E_p$  and  $E_n$  for the protons and neutrons knocked out from the  $1s_{1/2}$  and  $1p_{1/2}$  shells. The calculations were performed with the standard set of the Skyrme forces (S1–S6). Our experimental points are also plotted in Fig. 4. The comparison of the theory with the experiment allows to reject the Skyrme forces

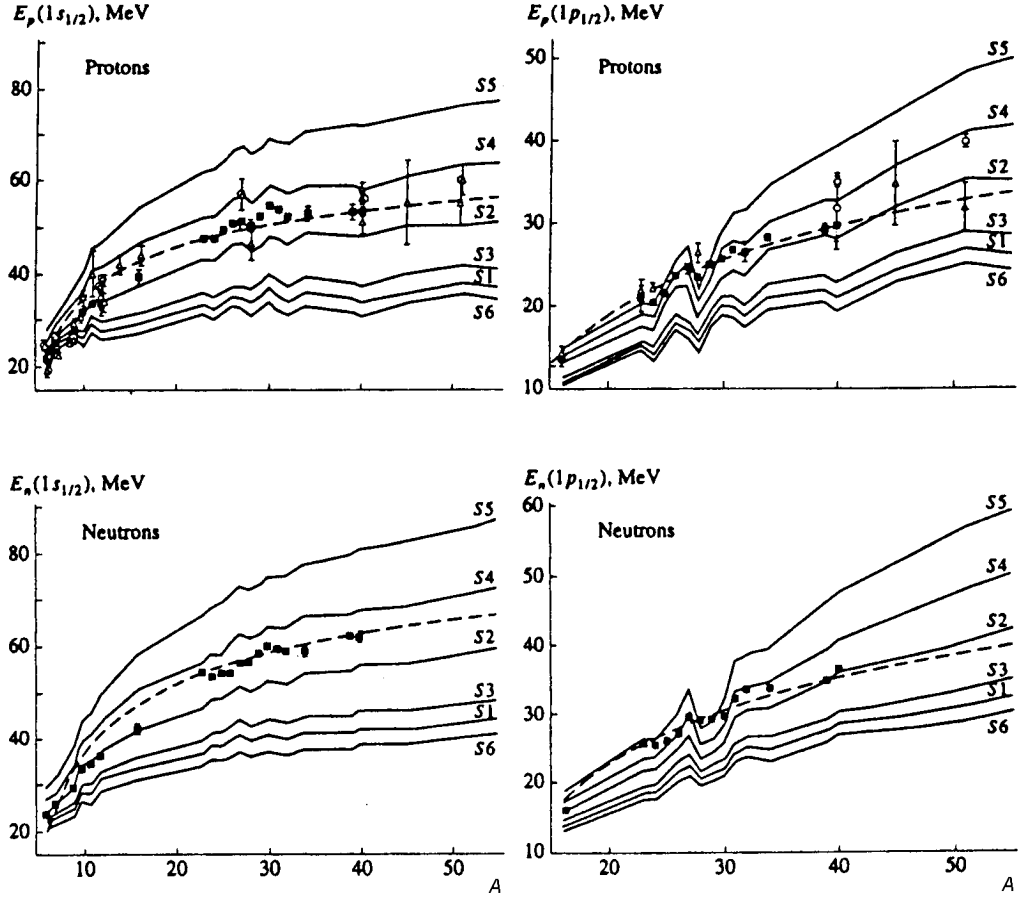


Fig. 4. The  $A$ -dependence of the single-particle binding energies of the protons and neutrons in the  $1s_{1/2}$  and  $1p_{1/2}$  states. Here  $\blacksquare$ ,  $\circ$ , and  $\triangle$  show our results, the earlier data on  $(p, 2p)$  scattering, and the data on  $(e, e'p)$  scattering, respectively.

with small nonlocality (S6, S1, S3 with the ratio of the effective nucleon mass to the real one  $m^*/m = 0.96-0.76$ ). These forces lead to underestimation of the potential depth, also they do not describe the shell splitting due to nuclear deformation. Unfortunately, neither of the remaining versions can well describe simultaneously both the surface and the deep-lying energy levels. Preference may be given to the S4 version ( $m^*/m = 0.47$ ) or to the S2 version ( $m^*/m = 0.58$ ). Such ambiguity in the choice of the effective  $NN$  interaction is typical for the Hartree-Fock-Skyrme model. In spite of this shortcoming, the Hartree-Fock method with a fixed set of phenomenological parameters proved to be able to describe, at least qualitatively, the discussed above nuclear shell structure in a wide range of nuclear masses.

The analysis of the differential cross sections have been performed in DWIA with Hartree-Fock-Skyrme single-particle wave functions. The distortions of the wave functions of the outgoing and incident nucleons were calculated by the partial-wave and Glauber methods. The results of the DWIA calculations of the differential cross sections of the  $(p, 2p)$  and  $(p, np)$  reactions on  $^{16}\text{O}$  are presented in Fig. 5.

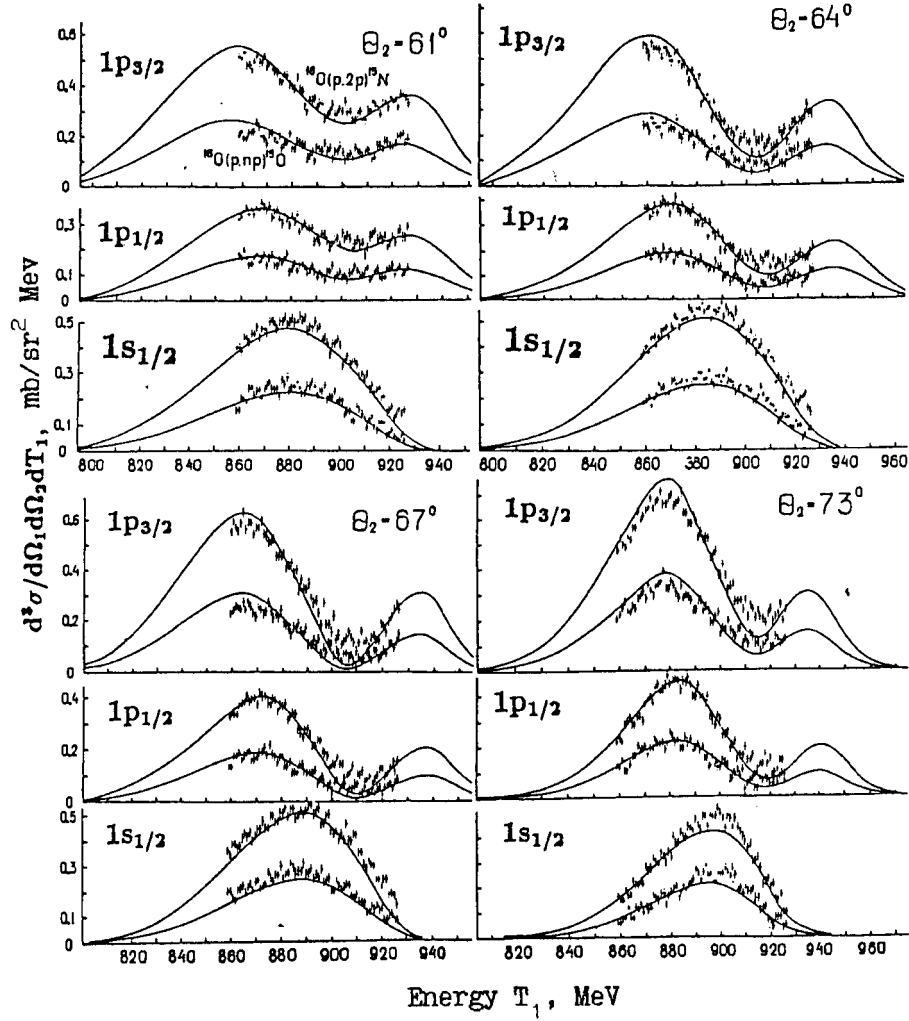


Fig. 5. Differential cross sections of quasielastic  $(p, 2p)$  and  $(p, np)$  reactions on  $^{16}\text{O}$ .  $T_1$  is the energy of the scattered proton. Solid lines represent calculated cross sections.

The reasonable agreement with the experiment allows to believe that the mechanism of the  $(p, Np)$  reactions, as well as the nuclear structure, are described in the used approach quite reliably. Similar conclusion can be drawn from the analysis of the differential cross sections of the knockout reactions on  $^{40}\text{Ca}$  (Fig. 6). Such good description of the **absolute**  $(p, 2p)$  and  $(p, np)$  cross sections means that the ratio of these cross sections should be described even more reliably, since the distortions of the nucleon waves in the  $(p, 2p)$  and  $(p, np)$  reactions are nearly the same.

Our experiment was specially designed in such a way that both the  $(p, 2p)$  and  $(p, np)$  reactions were detected simultaneously and in identical way. For analysis of the data we introduced the relative structure function

$$R_A(T_1) = [d^3\sigma_\nu/d\Omega^2 dT_1]_{A(p,np)} / [d^3\sigma_\nu/d\Omega^2 dT_1]_{A(p,2p)} \times [d\sigma/d\Omega]_{pp} / [d\sigma/d\Omega]_{pn}, \quad \nu = [n, l, j].$$

Experimentally, this function is determined as the ratio of the neutron to proton differential yields from a  $\nu$ -shell of the nucleus  $A$  normalized to the similar ratio measured on deuteron

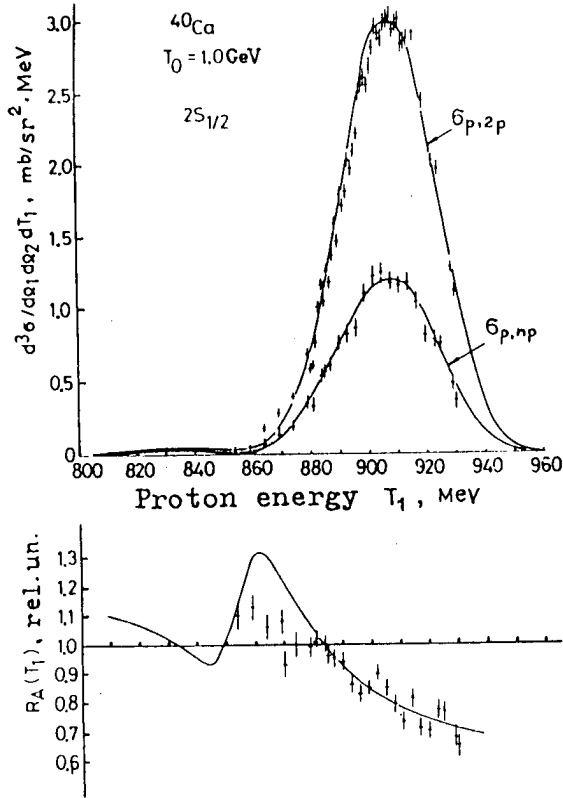


**Fig. 6.** Differential cross sections of quasielastic proton and neutron knockout and the relative structure function  $R_A(T_1)$  for  $2s_{1/2}$  shell of  $^{40}\text{Ca}$ . The curves are the result of calculation within the framework of DWIA with Hartree–Fock wave functions. The calculated shape of  $R_A(T_1)$  corresponds to  $r_n - r_p = -0.07$  fm for  $2s_{1/2}$  shell.

target. Thus introduced ratio has no systematic errors in absolute normalization and reflects explicitly the nuclear shell structure. It is mainly determined by the single-particle neutron and proton wave functions. The value and the sign of  $R_A(T_1)$  depend on the ratio of neutron to proton r.m.s. radii of nuclear shells. Using for estimations the harmonic oscillator wave functions, one can show within the PWIA that  $R_A(T_1) \simeq [\langle r_\nu^2 \rangle_n^{1/2} / \langle r_\nu^2 \rangle_p^{1/2}]^{2l+3}$ , where  $l$  is the nucleon orbital momentum. As a result, the measurement of the ratio  $R_A(T_1)$  appears to be the most sensitive method for investigation the differences in the r.m.s. radii of the proton and neutron distributions. Fig. 6 demonstrates that the difference  $r_n - r_p = -0.07$  fm was reliably detected in  $^{40}\text{Ca}$  in agreement with the Hartree–Fock calculations. Similar result was obtained in the analysis of  $^{16}\text{O}$ .

In the case of  $^{12}\text{C}$  the description of the absolute  $(p, 2p)$  and  $(p, np)$  cross sections was less successive as one can see from Fig. 7. Fig. 8 shows the measured ratio  $R_A(T_1)$  for this case as well as the calculated ratio. Note that the Hartree–Fock single-particle wave functions in  $^{12}\text{C}$  correspond to  $r_p$  being slightly larger than  $r_n$ . One can see from Fig. 8 that the experimental data do not agree with such assumption. However, the agreement with experiment can be reached assuming  $\langle r_\nu^2 \rangle_n^{1/2} / \langle r_\nu^2 \rangle_p^{1/2} \simeq 1.05$ .

These examples demonstrate how powerful is the relative structure function method in studying differences in the proton and neutron distributions in nuclear shells.

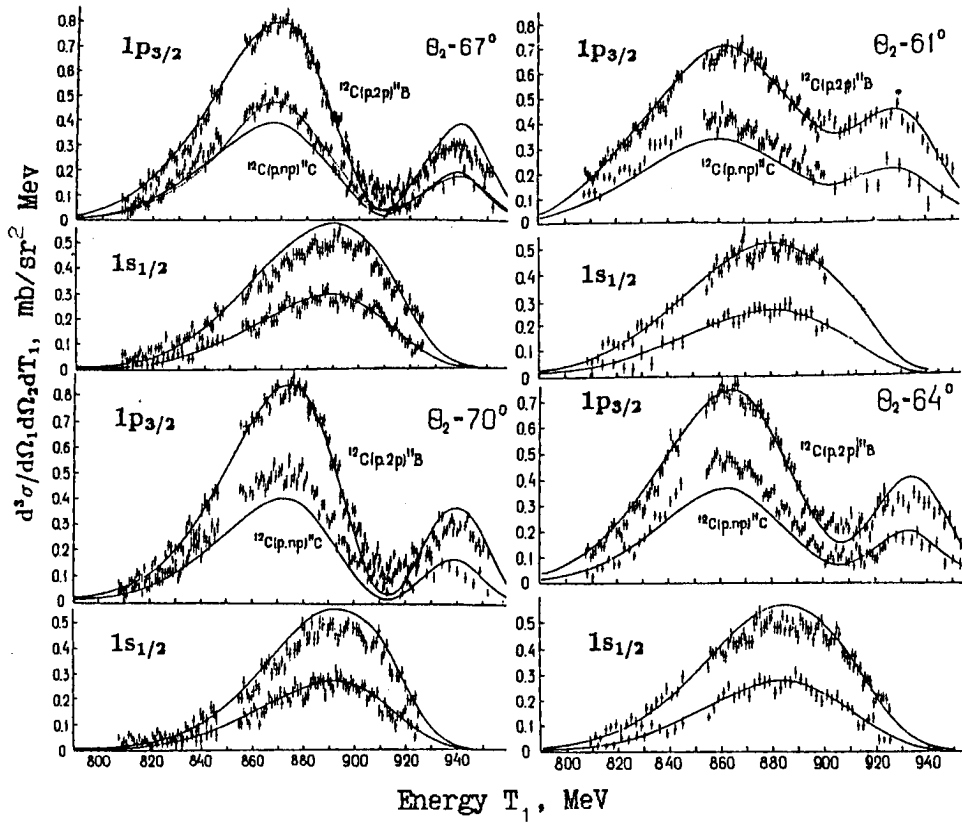


Fig. 7. Differential cross sections of quasielastic ( $p, 2p$ ) and ( $p, np$ ) reactions for  $^{12}\text{C}$ . Solid lines represent calculated cross sections.

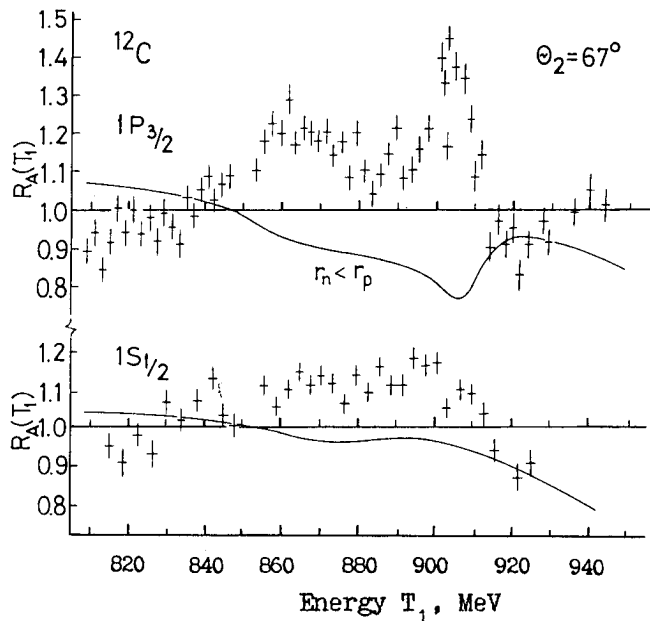


Fig. 8. Experimental and theoretical relative structure functions for  $^{12}\text{C}$ .

Concluding, we may point out that simultaneous studies of quasielastic ( $p, 2p$ ) and ( $p, np$ ) scattering on nuclei yielded valuable information on separation energies of the protons and neutrons. A large portion of experimental data on the neutron states and also on the deep-lying proton states has been obtained for the first time. The analysis of the fine structure of the spectra enabled us to determine principal characteristics of the deformed nuclear density, including previously unknown quadrupole moments of the neutron distributions. It is worth to note also the high sensitivity of such experiments to the differences in the proton and neutron r.m.s. radii. The obtained data can serve as a solid basis for testing the existing nuclear models and for developing new theoretical approaches to the microscopic descriptions of the nuclear structure.

## References

- [1] *S.L.Belostotsky, S.S.Volkov, A.A.Vorobyov, Yu.V.Dotsenko, L.G.Kudin, N.P.Kuropatkin, A.A.Lobodenko, O.V.Miklukho, V.N.Nikulin, O.E.Prokofiev.* // *Yad. Fiz.*, 1985. V.41. P.1425.
- [2] *Yu.V.Dotsenko, V.E.Starodubsky.* // *Yad. Fiz.*, 1985. V.41. P.107.
- [3] *S.L.Belostotsky, Yu.V.Dotsenko, N.P.Kuropatkin, O.V.Miklukho, V.N.Nikulin, O.E.Prokofiev, Yu.A.Scheglov, V.E.Starodubsky. A.Yu.Tsaregorodtsev, A.A.Vorobyov, M.B.Zhalov.* // *Proc. Int. Symp. on Mod. Develop. Nucl. Phys.*, Novosibirsk, 1987. P.191.
- [4] *Yu.V.Dotsenko, J.A.Chakhalyan, O.A.Domchenkov, N.P.Kuropatkin, A.A.Lobodenko, O.V.Miklukho, Yu.A.Scheglov, V.E.Starodubsky, A.Yu.Tsaregorodtsev, S.S.Volkov, A.A.Vorobyov.* // *Proc. Conf. on Selected Topics in Nuclear Structure*, Dubna, 1989. V.2. P.28.
- [5] *S.S.Volkov, A.A.Vorobyov, O.A.Domchenkov, Yu.V.Dotsenko, N.P.Kuropatkin, A.A.Lobodenko, O.V.Miklukho, V.N.Nikulin, V.E.Starodubsky, A.Yu.Tsaregorodtsev, J.A.Chakhalyan, Yu.A.Scheglov.* // *Yad. Fiz.*, 1990. V.52. P.1339.
- [6] *A.A.Vorobyov, Yu.V.Dotsenko, A.A.Lobodenko, O.V.Miklukho, I.I.Tkatch, L.N.Uvarov, A.Yu.Tsaregorodtsev, J.A.Chakhalyan, Yu.A.Scheglov.* // *Yad. Fiz.*, 1994. V.57. P.3.
- [7] *A.A.Vorobyov, Yu.V.Dotsenko, A.A.Lobodenko, O.V.Miklukho, I.I.Tkatch, A.Yu.Tsaregorodtsev, J.A.Chakhalyan, Yu.A.Scheglov.* // *Yad. Fiz.*, 1995. V.58. P.1923.